Available online at www.sciencedirect.com
SCIENCE DIRECT®
International Journal of Heat and Mass Transfer 49 (2006) 187–197
International Journal of HEAT and MASS TRANSFER
www.elsevier.com/locate/ijhmt

Implementation of an analytical two-dimensional inverse heat conduction technique to practical problems

P.L. Woodfield [a,1], M. Monde [b,*], Y. Mitsutake [b,2]

[a] Institute of Ocean Energy, Saga University, 1 Honjo-machi, Saga 840-8502, Japan
[b] Department of Mechanical Engineering, Saga University, 1 Honjo-machi, Saga 840-8502, Japan

Received 4 March 2005
Available online 27 September 2005

Abstract

Two improvements to practical implementation of a solution to the two-dimensional inverse heat conduction problem are presented. The first concept is useful for experimental data with strong or irregular fluctuations in time. The second procedure improves the spatial resolution for problems where the source of the surface heat flux distribution is moving along the surface. The method is tested against analytical solutions and data from quench cooling experiments. Both procedures are found to enhance the quality of the inverse solution results.

Keywords: Inverse heat conduction; Analytical solution; Implementation

1. Introduction

Explicit analytical solutions [1–7] for inverse heat conduction problems (IHCP) have an advantage over many other methods in that solutions can be obtained quickly without iteration. They are most useful in cases where the geometry is simple, which often occurs in fundamental experimental investigations relating to heat transfer where for practical reasons the temperature sensors cannot be placed directly on the surface. In boiling heat transfer research [8,9] the surface morphology has a direct influence on the phenomenon of interest making inverse solutions extremely useful. Other important applications for IHCP solutions include controlled cooling of electronic components [10], estimation of thermal deformation in machine tools during operation [11] and determination of conditions at the interface between the mold and metal during metal casting [12].

Recently Monde et al. [1–4] successfully demonstrated a new analytical procedure for predicting surface temperature and heat flux based on temperature measurements within the solid. The novelty of their work was the use of a polynomial series in the half power of time to approximate the measured data. In implementing the method to experimental data we have found that a number of practical issues can arise that influence the quality of the final solution. In this article we present some innovations relating to how to apply the method

* Corresponding author. Tel.: +81 952 28 8608; fax: +81 952 28 8587.
E-mail addresses: peter@me.saga-u.ac.jp (P.L. Woodfield), monde@me.saga-u.ac.jp (M. Monde), mitutake@me.saga-u.ac.jp (Y. Mitsutake).
[1] Tel.: +81 952 26 3870; fax: +81 952 28 8595.
[2] Tel.: +81 952 28 8616; fax: +81 952 28 8587.

0017-9310/$ - see front matter © 2005 Elsevier Ltd. All rights reserved.
doi:10.1016/j.ijheatmasstransfer.2005.06.035

Nomenclature

a	thermal diffusivity
$C_{j,k}$	coefficient defined by Eq. (A.1)
$F_j(t)$	coefficient of jth eigenfunction as a function of time
$J_0(\ )$	zero order Bessel function of the first kind
l	wavelength of cosine function for Eq. (13)
m_j	jth eigenvalue
$m_{j\text{cut}}$	'cut-off' eigenvalue for Eq. (11)
N_j	number of eigenvalues minus 1
N_k	number of terms in approximating polynomial minus 1
$P_{j,k}$	coefficient of function to approximate measured temperature
q_0	magnitude of oscillating heat flux boundary condition
r	radial coordinate
R	radius of domain
s	Laplace domain variable
t	time
t^*	shifted zero time point
t_i	time for the ith measured data point of the experiment
t_{ni}	time at which the last data point was measured in the experiment
Δt	time period of oscillation ($=2\pi/\omega$)
T	temperature
T_0	temperature at time zero
u	variable for integration of Eq. (12)
x	Cartesian coordinate along surface
X	width of domain for Cartesian coordinate case
z	axial coordinate or depth from surface
Greek symbols	
θ	temperature change from initial ($T - T_0$)
λ	thermal conductivity
ϕ	interpolation angle
ω	time frequency of oscillating boundary condition

to experimental data better. The techniques introduced are relevant to other inverse solution procedures and not only to the Monde method.

2. Overview of the Monde method

The aim of the present IHCP is to determine the surface temperature and heat flux distribution based on the readings of the temperature sensors at the positions shown in Fig. 1. Eq. (1) gives the unsteady heat conduction relation for cylindrical coordinates and the initial and boundary conditions are expressed in Eqs. (2a)–(2d).

$$\frac{1}{a}\frac{\partial T}{\partial t} = \frac{1}{r}\frac{\partial}{\partial r}\left(r\frac{\partial T}{\partial r}\right) + \frac{\partial^2 T}{\partial z^2} \tag{1}$$

$$T = T_0 \quad \text{at } t = 0 \tag{2a}$$

$$\frac{\partial T}{\partial r} = 0 \quad \text{at } r = R \quad \text{and} \quad r = 0 \tag{2b}$$

$$T - T_0 = \sum_{j=0}^{N_j} F_j^{(1)}(t) J_0\left(m_j \frac{r}{R}\right) \quad \text{at } z = z_1 \tag{2c}$$

$$T - T_0 = \sum_{j=0}^{N_j} F_j^{(2)}(t) J_0\left(m_j \frac{r}{R}\right) \quad \text{at } z = z_2 \tag{2d}$$

In Eqs. (2c) and (2d), $F_j^{(1)}(t)$ and $F_j^{(2)}(t)$ are polynomial functions of the half power of time with coefficients selected such that these equations approximate the measured temperature/time distribution at depths z_1 and z_2. The eigenvalue, m_j, is the jth positive root of $J_1(m_j) = 0$. Eq. (3) gives an example of the half-power polynomial function for the first depth in Fig. 1.

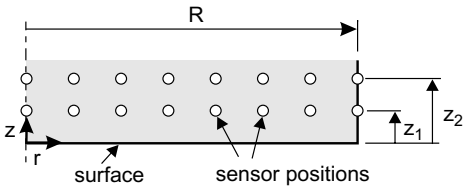

Fig. 1. Geometry of two-dimensional inverse heat conduction problem.

$$F_j^{(1)}(t) = \sum_{k=0}^{N_k} P_{j,k}^{(1)} t^{k/2} / \Gamma(1 + k/2) \tag{3}$$

The gamma function, $\Gamma(\ )$, is included in the denominator of Eq. (3) to make the form of the transformation to Laplace space a little more convenient. It should be noted here that the original work by Monde et al. [1] included a time lag in the half-power polynomial, which is not present in Eq. (3). The time lag can improve the result near time equals zero but for clarity of the discussion it is omitted in the present overview. It becomes redundant at larger times if the procedure suggested below in Section 3 is employed.

By substituting $\theta = T - T_0$ and taking Laplace transforms, Eqs. (1) and (2) can be solved in Laplace space to give Eq. (4). In this equation the over-bar represents the Laplace transformed version of the variable or function.

$$\bar{\theta}(r,z,s) = \sum_{j=0}^{N_j} J_0\left(m_j \frac{r}{R}\right)\bar{F}_j^{(1)}(s) \times \frac{\sinh\left(\sqrt{s/a + m_j^2/R^2}(z_2 - z)\right)}{\sinh\left(\sqrt{s/a + m_j^2/R^2}(z_2 - z_1)\right)} - \sum_{j=0}^{N_j} J_0\left(m_j \frac{r}{R}\right)\bar{F}_j^{(2)}(s) \times \frac{\sinh\left(\sqrt{s/a + m_j^2/R^2}(z_1 - z)\right)}{\sinh\left(\sqrt{s/a + m_j^2/R^2}(z_2 - z_1)\right)} \quad (4)$$

The Laplace transform of Eq. (3) results in Eq. (5).

$$\bar{F}_j^{(1)}(s) = \sum_{k=0}^{N_k} P_{j,k}^{(1)}/s^{(k+2)/2} \quad (5)$$

If we neglect all singularities except at $s = 0$ we can replace the fractions involving hyperbolic sine functions by power series expansions about $s = 0$ to obtain Eq. (6) (see Appendix A).

$$\bar{\theta}(r,s) = \sum_{j=0}^{N_j} J_0\left(m_j \frac{r}{R}\right)\left(\bar{F}_j^{(1)}(s)\sum_{k=0}^{\infty} C_{j,k}^{(2)} s^k - \bar{F}_j^{(2)}(s)\sum_{k=0}^{\infty} C_{j,k}^{(1)} s^k\right) \quad (6)$$

Multiplying $\bar{F}_j^{(1)}(s)$ by the power series expansion and retaining only terms that have s in the denominator, the temperature distribution in s-space (near $s = 0$) takes on the form given by Eq. (7).

$$\bar{\theta}(r,s) = \sum_{j=0}^{N_j} J_0\left(m_j \frac{r}{R}\right)\left(\sum_{k=-1}^{N_k} G_{j,k}^{(12)}/s^{(k+2)/2} - \sum_{k=-1}^{N_k} G_{j,k}^{(21)}/s^{(k+2)/2}\right) \quad (7)$$

The inverse Laplace transform of Eq. (7) can be found from tables of Laplace transforms [13] to give the surface temperature distribution as a function of time as in Eq. (8).

$$T(r,t) - T_0 = \sum_{j=0}^{N_j} J_0\left(m_j \frac{r}{R}\right)\left(\sum_{k=-1}^{N_k} G_{j,k}^{(12)} t^{k/2}/\Gamma(1 + k/2) - \sum_{k=-1}^{N_k} G_{j,k}^{(21)} t^{k/2}/\Gamma(1 + k/2)\right) \quad (8)$$

The surface heat flux distribution can be determined by differentiating Eq. (4) with respect to z and then proceeding in a similar manner. Further details of the above procedure can be found in Appendix A and in Refs. [1–4]. It is worth noting that to change Eq. (8) to Cartesian coordinates, the only alterations necessary are to replace $J_0(m_j r/R)$ with $\cos(m_j x/X)$ and set m_j equal to $j \times \pi$.

3. Application to large data sets with irregular time fluctuations

When the data has many irregular fluctuations in time it becomes impossible to use a polynomial with less than eight terms to approximate the whole range of the data accurately. Adding more terms to the polynomial does not solve the problem since numerical errors are introduced by the appearance of large positive and negative coefficients for the high-order terms. Previously, to overcome this problem, Monde divided the data into time partitions and then applied the half-polynomial series to the data within each partition separately [1]. By careful selection of the size, start and end position of each partition, the experimental data could be approximated well and accurate results could be obtained by the inverse solution. However, we have found that when processing many data sets it can become tedious to select appropriate positions for the partitions such that numerical overshoots in the solution do not appear near the start and end of the partitions. Moreover, for two-dimensional data, sudden changes in the cooling curves may not occur at exactly the same time for each radial position. This can introduce some ambiguity in a procedure to systematically select the start and end of each partition. For these reasons we have devised an alternative procedure as follows.

With unsteady heat conduction problems there is a general tendency for the solid temperature distribution to 'forget' the long-term history. In practice this means that it is not necessary to use all of the data to evaluate the temperature distribution at any given time, t. For the present study, at any given time, t, we use a small window of the data as illustrated in Fig. 2. As indicated in the figure, the minimum size for the window relates to the Fourier number based on the depth of the second thermocouple.

In a one-dimensional analysis it is safe to assume that the temperature distribution was uniform at a time t^* where the Fourier number, $a(t - t^*)/(z_2)^2 > 0.7$. The Fourier number of 0.7 results in a maximum error of less than 0.1% of the non-uniformity, MAX($|T - T_{av}|$), in the temperature distribution at time t^*. This arises because the transient factor in the leading term of solutions for the finite slab with controlled temperature boundaries is generally of the form $\exp(-\pi^2 at/L^2)$ where L is the thickness of the slab [13]. In other words, after a short period of time the factor, $\exp(-\pi^2 at/L^2)$ tends to become zero, the initial temperature distribution in the slab is 'forgotten' and the present distribution is the result of only the recent history of the temperature on the boundaries. Thus it is not necessary to include the

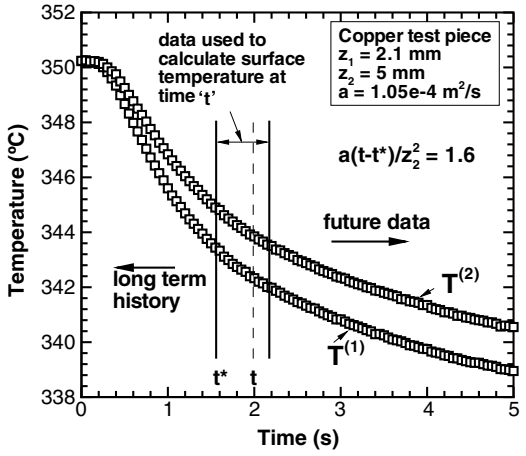

Fig. 2. 'Window' of data used to calculate surface temperature at time, 't'.

entire history from the experimental data so long as the boundary temperatures are approximated well and enough past information is included. For two-dimensional analysis it can be shown that in a similar manner, the minimum required Fourier number is of the order of 0.7 for 0.1% accuracy and 1.6 for 0.0001% accuracy.

Using this reasoning we can apply the equations in Section 2 for any time, t, by shifting the zero time position so that it is always at t^* where $a(t-t^*)/(z_2)^2$ is sufficiently large to justify neglecting the non-uniformity in the distribution at time t^*. For a direct solution it should be necessary to include data in the range from t^* to t only. For inverse solutions, however, it may be meaningful also to include some future data beyond time t in the curve-fit. The amount of future data should correspond to at least the time required for a sudden change in the surface temperature to be detected by the sensors at the first depth. In the present study, the experimental data used to calculate the surface temperature and heat flux at time t is all data that falls in the range from $t-1.6(z_2)^2/a$ to $t+0.8(z_2)^2/a$. This is illustrated in Fig. 2 for a copper test piece. The values, 1.6 and 0.8, for the Fourier numbers were selected since they satisfy the above-mentioned criteria. Also, some numerical experiments were performed to verify that this time range was not too large for the authors' experimental temperature measurements to be well approximated by a half-polynomial series. Thus in applying Eq. (8) to calculate the surface temperature, t is replaced by $t-t^*$ and each point in time is calculated separately by fitting Eq. (3) to a different 'window' of the original data. This is more computationally expensive than the time partition approach but it results in a consistent treatment that requires no special procedure to determine the position of the partitions.

4. Experimental data with varying thermal properties

An additional benefit becomes possible as a result of applying the solution to separate windows of the data. Fundamentally, the inverse solution assumes that the thermal properties of the solid are constant. However, for some applications thermal properties may vary significantly with temperature. Since each window of data is considered independently we only need to assume that the properties are constant for the duration of each window. Therefore if desired, a 'best estimate' of thermal properties can be obtained as a function of an average of the measured temperatures within the small time window of the data rather than for the whole data range. However, the effect of large spatial variations in thermodynamic properties cannot be accounted for in the present analytical solution.

5. Interpolation strategy for improving spatial resolution

Ideally, many temperature sensors should be used so that the number of eigenvalues, (N_j+1), in Eq. (8) can correspond exactly to the number of temperature sensors at each depth and sharp spatial resolution can be achieved. However, for practical reasons there is a limit to the number of thermocouples that can be placed in the solid. Thus to obtain good resolution, it becomes necessary to use an interpolation procedure so that not only the value of the temperature at the measuring points is considered but also the spatial and temporal trends of the data. This extra information extracted from the data allows the number of eigenvalues, (N_j+1), to be increased beyond the number of sensors. Practical implementation of this concept can be realized by interpolation of extra points between the measured positions and treating the interpolated data as additional 'measurement points'. Thus using only eight sensors and a cubic spline interpolation procedure it becomes possible to construct a 30-eigenvalue series [4].

Simply fixing the time and interpolating extra points in space was successfully employed by Hammad et al. [4] to reproduce a reasonably sharp step heat flux distribution based on computer generated temperature data for 16 points within the solid. However, in the case of a moving spike in the heat flux distribution such as may occur in quenching experiments, numerical peaks in the predicted heat flux distribution sometimes appear immediately above the temperature sensors. The numerical peaks can be removed by extra smoothing of the experimental data but this tends to lead to a large underestimate of the magnitude of the peak heat flux.

A better procedure is illustrated in Fig. 3 where for example, the temperature is being interpolated to the point 'A'. The aim is to include not only the spatial trend

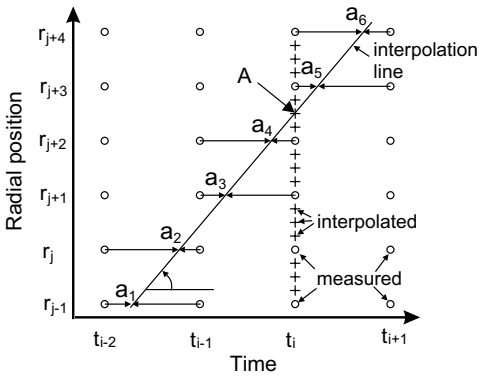

Fig. 3. Procedure for interpolating extra points to increase the maximum possible number of eigenvalues. Data is being interpolated to position 'A' at time, 't_i'.

but also the temporal trend in the interpolation. The angle ϕ is chosen so that $\tan(\phi)$ corresponds approximately to the prevailing direction of the temperature contours at time, t_i, which we interpret as the spatial averaged temperature/time gradient divided by the spatial averaged radial temperature gradient. Numerically $\tan(\phi)$ is calculated using finite differences as given in Eq. (9).

$$\tan(\theta_i) = \left| \overline{\left(\frac{\partial T}{\partial t}\right)} \Big/ \overline{\left(\frac{\partial T}{\partial r}\right)} \right| \approx \left| \sum_{j=2}^{nj-1} \frac{T_{i+1,j} - T_{i-1,j}}{t_{i+1} - t_{i-1}} \Big/ \sum_{j=2}^{nj-1} \frac{1}{2} \left(\frac{T_{i,j+1} - T_{i,j}}{r_{j+1} - r_j} + \frac{T_{i,j} - T_{i,j-1}}{r_j - r_{j-1}} \right) \right| \quad (9)$$

The physical reasoning behind using the interpolation procedure shown in Fig. 1 is that if the peak flux is moving in the positive radial direction, as in the case of a moving wetting front, then we may expect the temperature contours on a space/time plot also to move approximately in the same direction. We have found that interpolating parallel to the expected contour direction reduces the likelihood of non-physical peaks in surface heat flux appearing above the sensor locations.

Some numerical constraint is needed for the minimum value of $\tan(\phi)$ in Eq. (9) since very small angles can lead to numerical errors. In our computer program the minimum angle is controlled as given in Eq. (10). For this equation, $\tan(\phi_{\min})$ is a number smaller than the minimum observed wetting front velocity.

$$\tan(\phi_i) = \mathrm{MAX}(\tan(\phi_i), \tan(\phi_{\min})) \quad (10)$$

Having determined the slope of the interpolation line from Eqs. (9) and (10) for every time, t_i, near-neighbor averaging is used to smooth the slope so that noise in the data does not cause the slope to change dramatically each time step. Finally, for the example shown in Fig. 3, data is first interpolated to the points, a_1, a_2, a_3, etc. and then cubic splines are used to make the interpolation to the point 'A'.

6. Damping the coefficients of high frequency eigenfunctions

The coefficients of the higher frequency eigenfunctions in Eq. (3) are generally less accurate than the coefficients of the low frequency modes due to the uncertainties introduced by the interpolation procedure. Furthermore, it is possible that the interpolation will introduce some high frequency noise, which can ruin the quality of the inverse solution. For this reason damping of the higher frequency components is warranted. Eq. (11) gives the second-order Butterworth type smoother used in the present work applied to Eq. (3) at the measurement time t_i.

$$F_j^{(1)}(t_i)|_{\mathrm{smooth}} = F_j^{(1)}(t_i)|_{\mathrm{raw}} / (1 + (m_j/m_{j\mathrm{cut}})^4) \quad (11)$$

After some numerical experimentation, the 'cut-off' eigenvalue, $m_{j\mathrm{cut}}$ was taken to correspond to the number of thermocouples at each depth plus 3 (viz. $m_{j\mathrm{cut}} = m_{10}$ for eight thermocouples). In this way, the high frequency modes due to the interpolated data are strongly damped while the lower frequency data is gently smoothed.

7. Results

7.1. Effect of neglecting long-term history

The first test case is a one-dimensional inverse heat conduction problem where the exact solution is a triangle-wave function for heat flux at the surface. Temperature/time histories for two points, one at 2 mm below the surface and the second at a depth of 5 mm were generated using superposition of the one-dimensional analytical solutions for a ramp heat flux and a constant heat flux on the surface of a semi-infinite solid. The solid was taken to have the properties of copper and the peak heat flux of 1 MW/m^2 was chosen to correspond to the order of magnitude that appears in typical quench-cooling experiments using water. The triangle-wave function was selected since it is difficult to approximate the whole range of data with a polynomial series.

Fig. 4 gives the results of applying the present inverse solution procedure to the above problem. If the whole range of the data is used to determine the coefficients for Eq. (3) then the internal temperatures are not well approximated by the polynomial containing eight terms and a rather poor prediction of the heat flux results as is shown by the black symbols in Fig. 4a. If however, the

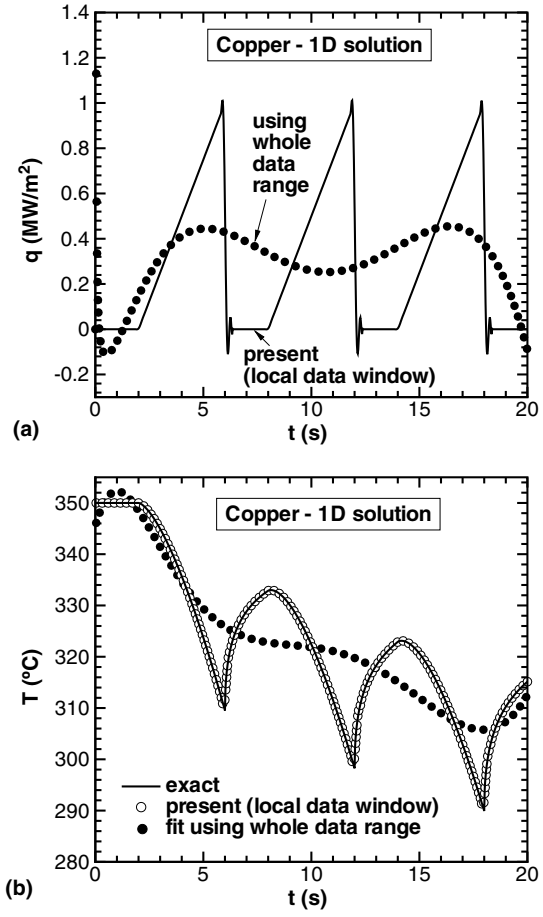

Fig. 4. Predicted (a) surface heat flux and (b) surface temperature for one-dimensional inverse problem where exact solution is a periodic triangle-wave heat flux.

heat flux is calculated using the present procedure, with a local window of the data, the triangle-wave function is well reproduced. Small overshoots appear near the discontinuities since the approximating function cannot perfectly resolve the sudden change in temperature shortly after the step change in heat flux. The predicted surface temperature is in excellent agreement with the analytical solution as shown in Fig. 4b.

7.2. Time resolution limit

Because of the thermal inertia of the solid, high frequency modes are strongly damped placing an upper limit to the frequency of the fluctuations that can be detected by sensors within the solid. This is illustrated in Eq. (12), which is the exact one-dimensional solution [13] for temperature within a semi-infinite solid with a sine wave heat flux boundary condition, $q_0\sin(\omega t)$, and an initial temperature of T_0.

$$T - T_0 = \frac{q_0}{\lambda}\sqrt{\frac{a}{\omega}}\mathrm{e}^{-z\sqrt{\omega/2a}}\sin\left(\omega t - z\sqrt{\omega/2a} - \pi/4\right) + \frac{2q_0 a\omega}{\pi\lambda}\int_0^\infty \frac{\cos(uz)}{\omega^2 + a^2u^4}\mathrm{e}^{-au^2t}\mathrm{d}u \qquad (12)$$

The first term on the right of Eq. (12) is the steady periodic part of the solution and the second term is a transient. From the form of the coefficient of the sine function in Eq. (12) it is clear that the magnitude of the oscillation diminishes quickly with depth into the solid and more so if the frequency is larger.

Eq. (12) provides a useful test case for the present procedure since the time resolution limit will depend also on the size of the window of data used for the polynomial fit in relation to the period of the oscillation ($2\pi/\omega$). The term involving the integral in Eq. (12) generally converges quickly and can be evaluated numerically to an arbitrary precision. Fig. 5 shows present predictions of the surface heat flux based on temperatures calculated with Eq. (12) at 2 mm and 5 mm beneath the surface of a copper block. The agreement between the exact result and the prediction is excellent for the lower frequency case of one cycle per second ($\omega = 2\pi$ radians/s). The accuracy of the predictions diminishes as the frequency increases.

From Fig. 5 it is apparent that the time resolution for the present calculation is limited to an oscillation with a time period, $\Delta t = 2\pi/\omega$, of about 0.3 s. In terms of the Fourier number this is $a\Delta t/z_2^2 \cong 1.3$. It is worth noting that this number is smaller than the window of data $(1.5a(t - t^*)/z_2^2 = 2.4)$ used to calculate the surface heat

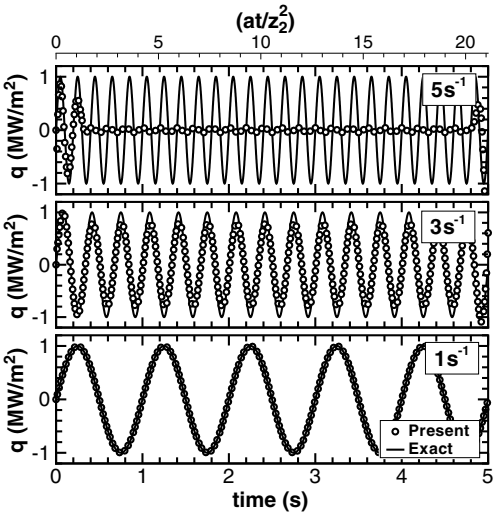

Fig. 5. Surface heat flux for one-dimensional problem where exact solution is a sine wave (copper, $z_1 = 2$ mm, $z_2 = 5$ mm).

flux in the inverse solution. We have found that reducing the size of the data window improves the time resolution for the case in Fig. 5. However, this is at the risk of introducing some error by neglecting some of the more recent thermal history for the solid. So in order to resolve data with significant higher frequency time components it may be necessary to reach a compromise between two factors. The first is the limitation of the truncated polynomial series for mapping strong fluctuations and the second is inaccuracy due to over-restriction of the amount of data used in the calculation. Nevertheless, it is important to keep in mind that Eq. (12) shows that the amplitude of the oscillation that would be detected by the sensor 2 mm beneath the copper surface for a frequency of 5 s^{-1} is only 2.2 K and at 5 mm it is less than 1 K for the present example. Also we do not want the polynomial to follow higher frequency noise in the data, which is one of the advantages of using a least-squares polynomial fit.

In summary, the depth of the sensors beneath the surface, the magnitude of the heat flux, the accuracy of the sensor and the size of the window of data used for the inverse solution influence the time resolution limit.

7.3. Effect of spatial interpolation procedure

To illustrate the improvement to predictions resulting from the spatial interpolation procedure and the applicability of the method to experimental data we have applied the method to two experimental cases and one set of computer-generated data.

The first example using two-dimensional experimental data is from Hammad et al. [8] for jet impingement quench-cooling. Fig. 6 compares two different procedures for interpolating additional points between the measured data. In the experiment, temperatures were measured at two depths with eight thermocouples at each depth. For the present calculation 28 eigenvalues are used and the half-power polynomial series has eight terms. Fig. 6a gives the calculated surface heat flux using the procedure outlined in Section 3 above. Fig. 6b gives the results obtained by fixing time and interpolating in space. This is equivalent to setting ϕ to $\pi/2$ in Fig. 3. Clearly in Fig. 6b, localized peaks appear along the line of maximum heat flux. The peaks appear above the locations of the temperature sensors. This problem is overcome using the present procedure as is shown in Fig. 6a.

The second example of application of the procedure to experimental data is shown in Fig. 7. This case is for a falling film of liquid water onto a steel block 100 mm long and 50 mm deep. Thermocouples are placed at 2 mm and 5 mm beneath the surface and are spaced approximately 10 mm apart. This case differs from Fig. 6 in that Cartesian coordinates are used, the material is steel and the spacing between thermocouples is greater. Fig. 7a shows the surface heat flux distribution estimated using the present interpolation procedure, while Fig. 7b shows results from interpolating by fixing the time. Again non-physical peaks appear above the thermocouple locations in Fig. 7b. A notable improvement to this problem is again achieved by the present procedure as illustrated in Fig. 7a.

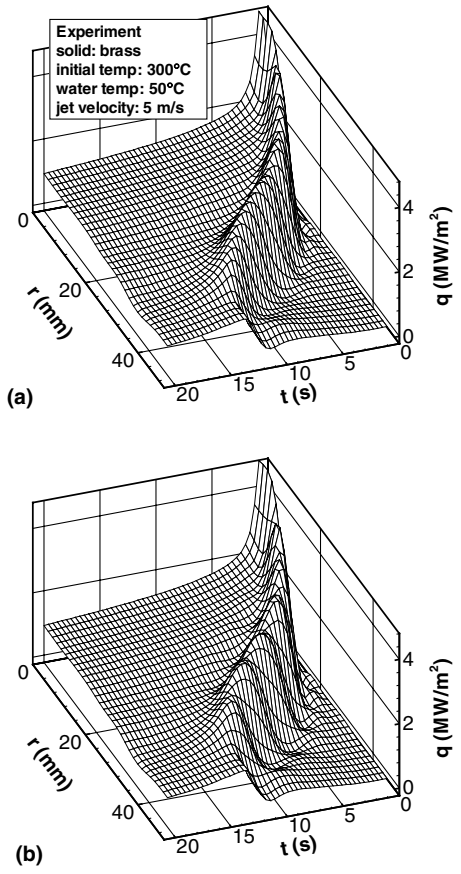

Fig. 6. Surface heat flux distribution calculated from experimental data for an impinging jet experiment [8]: (a) present and (b) fixed time interpolation.

To verify the accuracy of the method, we have also considered computer-generated data for a moving annular step source of surface heat flux. The width of the step is set a little larger than the spacing of the temperature sensors and the step moves at a constant velocity in the radial direction. Fig. 8 gives the calculated surface heat flux distribution for this problem using the present method and fixed time interpolation. The effect is the same as is shown in Figs. 6 and 7 verifying that the peaks in Figs. 6 and 7 are certainly due to the interpolation procedure and not some physical phenomenon from the experiment.

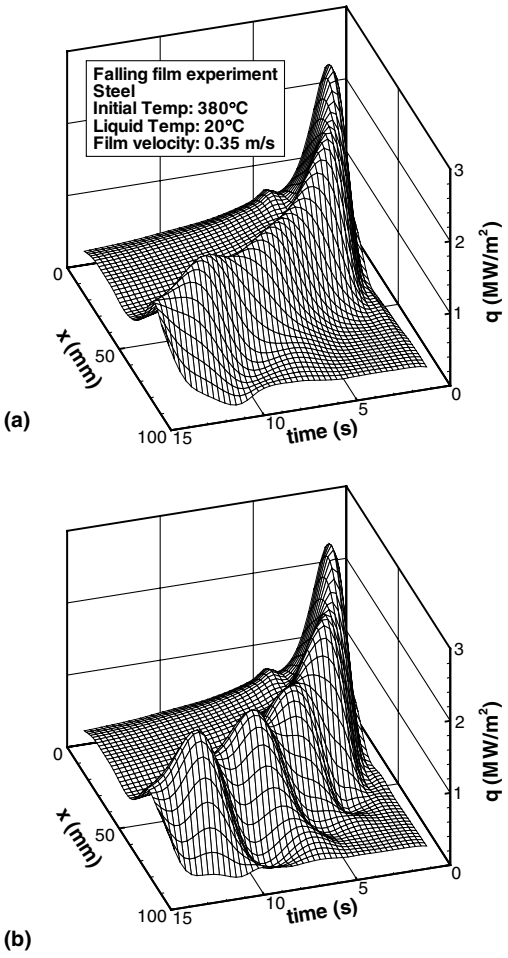

Fig. 7. Surface heat flux distribution calculated using data from falling film experiment: (a) present and (b) fixed time interpolation.

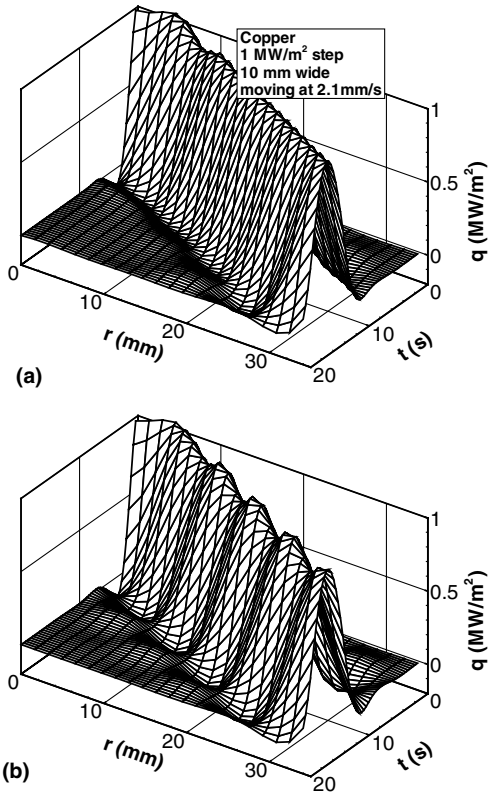

Fig. 8. Surface heat flux distribution for a moving rectangular step calculated based on computer generated data: (a) present and (b) fixed time interpolation.

7.4. Space resolution limit

It may be noticed in Fig. 8 that the peak heat flux of 1 MW/m^2 is reasonably well predicted by the present procedure. However, it is generally found for this kind of problem that if the width of the step is smaller than the thermocouple spacing the peak heat flux is under-predicted. Thus we cannot expect that the present method will give a better spatial resolution of heat flux than the physical spacing of the temperature sensors. However, the spatial resolution is certainly improved from that obtained using no interpolation and the same number of eigenvalues as measurement positions. Fig. 9 gives calculations of the instantaneous heat flux profile at a time of 10 s after the step moved from the center for three different step widths. Fig. 9a shows the cases where only eight eigenvalues were used, while Fig. 9b shows the present procedure with 28 eigenvalues. In all cases for Fig. 9, the number of sensors was eight. Generally the estimate of the peak heat flux is closer to the true value in Fig. 9b than in Fig. 9a. Concerning the shape of the distribution in Fig. 9, it is worth noting that the space resolution not only influences the magnitude of the peak heat flux but also the calculated shape. High frequency components contributing to the sharp profile of the exact heat flux distribution on the surface cannot be resolved properly. Thus the inverse solution does not follow the rectangular shape for heat flux in Figs. 8 and 9.

Fig. 10 compares the estimated surface temperature distributions with the exact values corresponding to the conditions and procedure for Fig. 9b. Again the predictions are better for the steps that are wider than the spacing of the sensors. Generally the inverse solution predictions for surface temperature appear better than the corresponding predictions for heat flux. This is a consequence of the fact that the higher frequency eigenfunctions make a smaller contribution to temperature than to heat flux.

From a numerical point of view we might expect that the spatial resolution can be improved simply by adding more sensors. This is illustrated in Fig. 11 where 15 sensors have been employed at each depth. In this case the

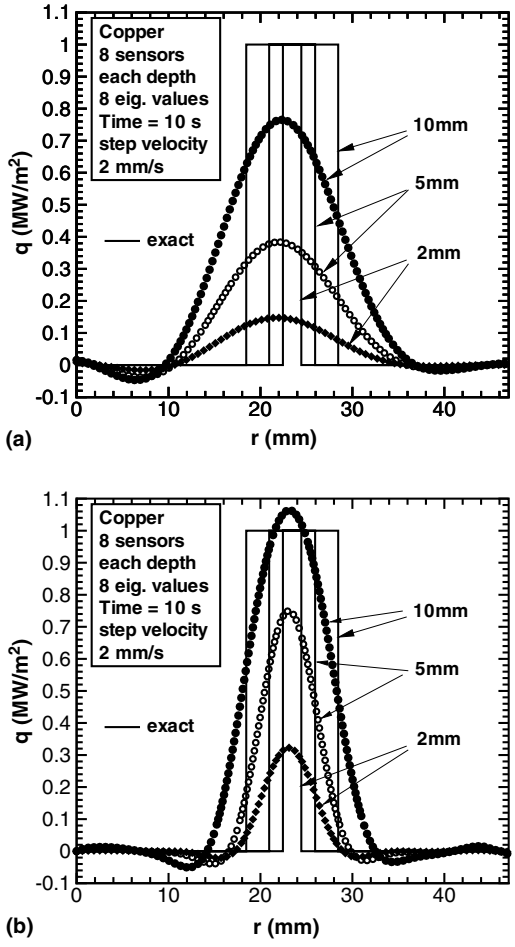

Fig. 9. Radial heat flux distribution for a moving rectangular step of different step widths (sensor spacing 6.7 mm): (a) no interpolation and (b) present interpolation method.

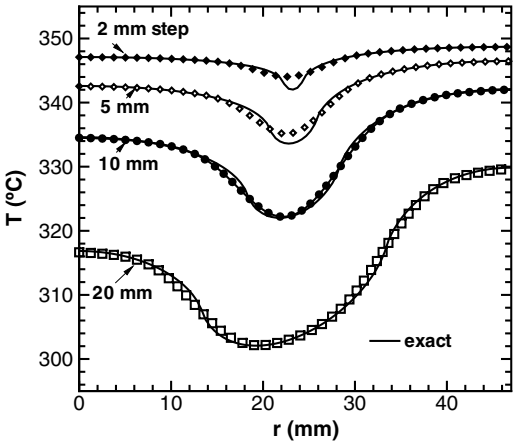

Fig. 10. Instantaneous radial temperature distribution for a moving rectangular step of different step widths. Symbols are results for present method using eight sensors and 28 eigenvalues.

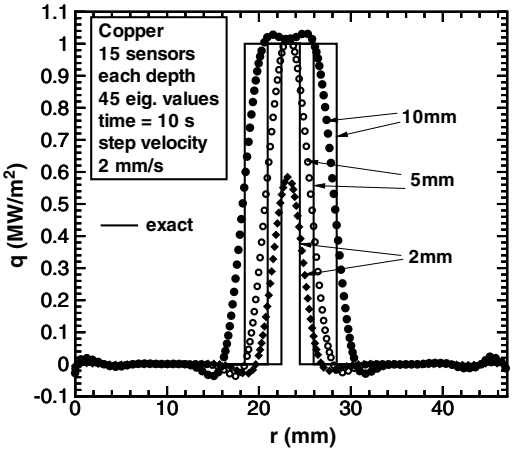

Fig. 11. Heat flux distribution showing effect of increasing number of sensors to 15 at each depth (sensor spacing 3.4 mm).

resolution is much better than that shown in Fig. 9b. However, it should be noted that the sensor spacing is not the only factor to be considered in determining the spatial resolution limit. Even if the sensor is infinitely small, the spatial resolution at the surface will be limited by experimental noise, the accuracy of the sensor and its depth beneath the surface.

Consider a simple steady-state case of a semi-infinite two-dimensional solid with a steady heat flux distribution in the shape of a cosine wave at the surface. Eq. (13) defines this problem.

$$\frac{\partial^2 T}{\partial x^2}+\frac{\partial^2 T}{\partial z^2}=0 \qquad (0\leqslant z<\infty,\ -\infty<x<\infty) \tag{13a}$$

$$-\lambda\frac{\partial T}{\partial z}\Big|_{z=0}=q_0\cos(2\pi x/l) \qquad (z=0,\ -\infty<x<\infty) \tag{13b}$$

$$T|_{z\to\infty}=T_\infty \tag{13c}$$

In Eq. (13), T is the temperature at any point in the solid, q_0 is the amplitude of the cosine-wave heat flux distribution at the surface, l is the wavelength, x is the spatial coordinate along the surface and z is the depth beneath the surface. The steady-state case is a useful illustration for considering space resolution since time resolution issues are not involved. In addition, the choice of a cosine function for the boundary condition (Eq. (13b)) is helpful since the eigenfunctions for the solution to the IHCP in rectangular coordinates are also cosine functions. The analytical solution to Eq. (13) is given in Eq. (14).

$$T-T_\infty=\frac{q_0 l}{2\lambda\pi}\mathrm{e}^{-2\pi z/l}\cos\left(\frac{2\pi x}{l}\right) \tag{14}$$

The amplitude of the resulting spatial cosine wave fluctuation in temperature will diminish with depth in the solid as indicated by the coefficient of the cosine function in Eq. (14). The effect will be stronger if the wavelength, l, is smaller. This implies that spatial modes beyond a certain frequency will become undetectable no matter how closely real sensors are placed in the x direction for a given depth, z, beneath the surface.

For an example, consider a practical case where the accuracy of the sensor is 0.1 K, the material is copper and the first thermocouple is 2.0 mm beneath the surface. Eq. (14) tells us a surface heat flux in the form of a cosine function with a wavelength of around 4.4 mm and amplitude of 1 MW/m^2 will not produce a detectable change in temperature at a depth greater than 2.0 mm from the surface. In other words if there is no restriction on sensor spacing, we may expect that the space resolution limit will be defined by a minimum detectable wavelength for the eigenfunction which is estimated to be of the order of 4.4 mm for the present example. Using eigenfunctions with shorter wavelengths than this in the inverse solution may not be meaningful. Finally, it should be noted that unlike the cosine function, Bessel functions do not have a fixed 'wavelength'. However, the peaks of $J_0(x)$ do appear approximately at an interval of 2π and the orders of magnitude should be the same in both cylindrical and Cartesian coordinates.

8. Conclusions and closing

Two innovations for application of the two-dimensional Monde method to experimental data were presented. The first represented an improvement for applying the procedure to data with strong or irregular fluctuations in time. The second is most useful for circumstances where the source of the surface heat flux is moving in the spatial direction. This circumstance can occur in quenching experiments with a moving wetting front. It is also demonstrated that the spatial resolution for the surface heat flux estimate is limited by the sensor spacing, the depth beneath the surface and the accuracy of the sensor.

Finally, the authors are pleased to make available openly the software developed for implementing the present inverse solution. Interested readers should contact the Monde laboratory at Saga University.

Appendix A. Details of coefficients for Eq. (8)

It is worthwhile to briefly describe a procedure for evaluating the coefficients in the inverse solution.

A.1. Expansion of hyperbolic sine functions

The mathematical step between Eqs. (4) and (6) is perhaps the most tedious part of the present procedure. We seek to find coefficients, $C^{(1)}_{j,k}$ such that Eq. (A.1) is accurately approximated in the vicinity of $s = 0$.

$$\sum_{k=0}^{\infty} C^{(1)}_{j,k} s^k = \sinh\left(\sqrt{s/a + m_j^2/R^2}(z_2 - z)\right) \Big/ \sinh\left(\sqrt{s/a + m_j^2/R^2}(z_2 - z_1)\right) \tag{A.1}$$

Using a Taylor series expansion it is possible to directly evaluate the coefficients in Eq. (A.1), however, the differentiation becomes very awkward as k becomes large. A slightly simpler approach is to expand both the numerator and denominator as separate series about $s = 0$. This is given in Eq. (A.2).

$$\sum_{k=0}^{\infty} C^{(1)}_{j,k} s^k = \sum_{p=0}^{\infty} \alpha_p s^p \Big/ \sum_{q=0}^{\infty} b_q s^q \tag{A.2}$$

where

$$\sum_{p=0}^{\infty} \alpha_p s^p = \sinh\left(\sqrt{s/a + m_j^2/R^2}(z_2 - z)\right) \tag{A.3}$$

$$\sum_{q=0}^{\infty} b_q s^q = \sinh\left(\sqrt{s/a + m_j^2/R^2}(z_2 - z_1)\right) \tag{A.4}$$

Using Taylor series expansions α_p and b_q can be evaluated without great difficulty. For example, for Eq. (A.3) we have

$$\alpha_p = \left(\frac{1}{p!}\frac{\mathrm{d}^p}{\mathrm{d}s^p}\left(\sinh\left(\sqrt{s/a + m_j^2/R^2}(z_2 - z)\right)\right)\right)\Big|_{s=0} \tag{A.5}$$

Noting that at the solid surface $z = 0$ and evaluating Eq. (A.5) where $s = 0$ gives us for example

$$\begin{aligned} \alpha_0 &= \sinh(z_2 m_j/R) \\ \alpha_1 &= \frac{z_2}{2a}\frac{R}{m_j}\cosh(z_2 m_j/R) \\ \alpha_2 &= \frac{z_2^2 R^2}{8a^2 m_j^2}\sinh(z_2 m_j/R) - \frac{z_2 R^3}{8a^2 m_j^3}\cosh(z_2 m_j/R) \end{aligned} \tag{A.6}$$

In general α_p is found to be of the form given by Eq. (A.7).

$$\alpha_p = \frac{1}{a^p p!}\left(\sum_{i=0}^{2p-1} \beta_{p,i}(R/m_j)^i \sinh(z_2 m_j/R) + \sum_{i=0}^{2p-1} D_{p,i}(R/m_j)^i \cosh(z_2 m_j/R)\right) \tag{A.7}$$

The coefficients, $\beta_{p,i}$ and $D_{p,i}$ can be determined in a computer program by the following formulae.

$$\beta_{p,i} = (1 - i/2)\beta_{p-1,i-2} + (z_2/2)D_{p-1,i-1} \quad \text{(A.8a)}$$

$$D_{p,i} = (1 - i/2)D_{p-1,i-2} + (z_2/2)\beta_{p-1,i-1} \quad \text{(A.8b)}$$

What remains is to determine $C^{(1)}_{j,k}$ as a function of α_p and b_q. This can be done by multiplying both sides of Eq. (A.2) by the series involving b_q and then equating coefficients. This results in the following recursive formulae:

$$C_{j,0} = \alpha_0/b_0 \quad \text{(A.9a)}$$

$$C_{j,k} = \frac{1}{b_0}\left(\alpha_k - \sum_{q=0}^{k-1} C_{j,q} b_{k-q}\right) \quad \text{(A.9b)}$$

It should be mentioned that for the special case where $m_j = 0$, appropriate coefficients for Eq. (A.2) can be determined simply by noting that

$$\sinh(x)/x = 1 + x^2/3! + x^4/5! + x^6/7! + \cdots \quad \text{(A.10)}$$

A.2. Final evaluation of coefficients, $G_{j,k}$, for Eq. (8)

The step between Eqs. (6) and (7) is not a major challenge. Multiplying the two series on the right hand side of Eq. (A.11) together and then equating the coefficients determines $G^{(12)}_{j,k}$.

$$\sum_{k=-1}^{N_k} G^{(12)}_{j,k}/s^{(k+2)/2} = \left(\sum_{p=0}^{N_k} P^{(1)}_{j,p}/s^{(p+2)/2}\right)\left(\sum_{q=0}^{(N_k+2)/2} C^{(2)}_{j,q} s^q\right) \quad \text{(A.11)}$$

Notice in Eq. (A.11) that the infinite series has been truncated to include only cases where s appears in the denominator. In a computer program, evaluation of $G^{(12)}_{j,k}$ can be done quite simply using the following algorithm denoted as Eq. (A.12).

$$\begin{aligned}
&\text{INITIALIZE} \quad G^{(12)}_{j,k} = 0 \quad (k = -1, N_k)\\
&\text{LOOP} \quad (p = 0, N_k)(q = 0, N_k)\\
&\text{IF } (q - (p+2)/2 < 0) \quad \text{THEN}\\
&G^{(12)}_{j,p-2q} = G^{(12)}_{j,p-2q} + P^{(1)}_{j,p} C^{(2)}_{j,q}\\
&\text{ENDIF}\\
&\text{ENDLOOP}
\end{aligned} \quad \text{(A.12)}$$

References

[1] M. Monde, H. Arima, W. Liu, Y. Mitutake, J.A. Hammad, An analytical solution for two-dimensional inverse heat conduction problems using Laplace transform, Int. J. Heat Mass Transfer 46 (2003) 2135–2148.

[2] M. Monde, H. Arima, Y. Mitsutake, Estimation of surface temperature and heat flux using inverse solution for one-dimensional heat conduction, J. Heat Transfer 125 (2003) 213–223.

[3] M. Monde, Analytical method in inverse heat transfer problem using Laplace transform technique, Int. J. Heat Mass Transfer 43 (2000) 3965–3975.

[4] J. Hammad, M. Monde, Y. Mitsutake, H. Arima, Determination of surface temperature and heat flux using inverse solution for two-dimensional heat conduction, Therm. Sci. Eng. 10 (2002) 17–26.

[5] O.R. Burggraf, An exact solution of the inverse problem in heat conduction theory and applications, ASME J. Heat Transfer 86 (1964) 373–382.

[6] E.M. Sparrow, A. Haji-Sheikh, T.S. Lundgren, The inverse problem in transient heat conduction, ASME J. Appl. Mech. 31 (1964) 369–375.

[7] M. Imber, Temperature extrapolation mechanism for two-dimensional heat flow, AIAA J. 12 (8) (1974) 1089–1093.

[8] J. Hammad, Y. Mitsutake, M. Monde, Movement of maximum heat flux and wetting front during quenching of hot cylindrical block, Int. J. Therm. Sci. 43 (2004) 743–752.

[9] D.E. Hall, F.P. Incropera, R. Viskanta, Jet impingement boiling from a circular free-surface jet during quenching: Part 1—single-phase jet, J. Heat Transfer 123 (2001) 901–910.

[10] M. Janicki, M. Zubert, A. Napieralski, Application of inverse problem algorithms for integrated circuit temperature estimation, Microelectron. J. 30 (1999) 1099–1107.

[11] M.H. Attia, S. Fraser, M.O.M. Osman, On-line estimation of time-variant thermal load applied to machine tool structures using a s-domain inverse solution, Int. J. Mach. Tools Manufacture 39 (1999) 985–1000.

[12] F. Lau, W.B. Lee, S.M. Xiong, B.C. Liu, A study of the interfacial heat transfer between an iron casting and a metallic mould, J. Mater. Process. Technol. 79 (1998) 25–29.

[13] H.S. Carslaw, J.C. Jaeger, Conduction of Heat in Solids, Oxford University Press, 2003.